Parameters of Cloud Ice Particles Retrieved from Radar Data

VALERY MELNIKOV

Cooperative Institute for Mesoscale Meteorological Studies, University of Oklahoma, and NOAA/OAR/National Severe Storms Laboratory, Norman, Oklahoma

(Manuscript received 14 June 2016, in final form 21 November 2016)

ABSTRACT

The mean axis ratio (length/width) and the degree of orientation of cloud ice particles are retrieved from radar differential reflectivity (Z_{DR}) and the copolar correlation coefficient (ρ_{hv}) measured with the S-band WSR-88D radar. Hardware differential phases and amplifications in the polarimetric channels affect measured Z_{DR} and ρ_{hv} and are taken into consideration in the retrieval procedure. The retrieval is performed for particles in shapes of hexagonal prisms, which are closer to shapes of real cloud particles than frequently used spheroids. The median retrieved axis ratio for prisms is larger than that for spheroids. The statistical 1σ retrieval errors caused by fluctuations of radar returns are about 40% in areas of signal-to-noise ratios stronger than 10 dB. The values of the degree of orientation lie in an interval from 2° to 23°, which points to significant perturbations in the orientations of ice particles most likely caused by the wind field.

1. Introduction

Radars employing various polarimetric configurations are widely used in remote sensing of clouds (e.g., Matrosov et al. 2001; Mace et al. 2002; Hubbert et al. 2014a,b; Görsdorf et al. 2015; Kneifel et al. 2015). The most popular radar configuration is the one with simultaneously transmitted and received (STAR) waves with orthogonal polarizations. A method to retrieve the mean axis ratio (length/width) and the degree of orientation of ice cloud particles from measured differential reflectivity (Z_{DR}) and copolar correlation coefficient (ρ_{hv}) was proposed by Melnikov and Straka (2013) for antenna elevation angles lower than 7°. The Weather Surveillance Radar-1988 Doppler (WSR-88D) systems raise their antennas up to 20°, at which angular dependences of Z_{DR} and ρ_{hv} should be taken into consideration. Cloud radars and many weather radars scan elevations angles up to 90°. Herein, the retrieval approach is extended to any elevation angle (section 2).

STAR radars have system differential reflectivity biases and differential phases in transmit and receive because the signal paths in the two polarimetric channels are different (e.g., Zrnić et al. 2006; Cunningham et al. 2013; Ice et al. 2014). These system parameters affect measured Z_{DR} and ρ_{hv} and must be taken into consideration in retrieval procedures. Polarized waves propagating in clouds and precipitation experience attenuation and propagation differential phase shift, so the propagation effects should be considered as well (section 2).

Cloud areas with $Z_{\mathrm{DR}} > 4$ dB at low elevation angles contain platelike ice particles (Melnikov and Straka 2013). In situ measurements by Williams et al. (2015) showed that such areas, named category B, contain pristine platelike and dendritic crystals. At high elevation angles, Z_{DR} values from such particles are smaller than 4 dB, but it is possible to distinguish them from ice columns and needles. So, the retrieval procedure is applied for particles, the shapes of which can be determined from radar data (section 3).

The shapes of platelike ice particles are close to prisms (e.g., Pruppacher and Klett 1997, sec 10) although they are frequently approximated with spheroids in scattering problems. The latter approximation is used frequently because the scattering properties of spheroids are well known (e.g., Gossard and Strauch 1983, section 6.2; Doviak and Zrnić 2006, section 8.5.2.4; Bringi and Chandrasekar 2001, section A1.1). The scattering properties of ice prisms are obtained with numerical methods (e.g., Hong 2007; Liu 2008; Teschl et al. 2009, 2013). Westbrook (2014) obtained approximations of scattering shape factors for prisms. Spheroids and prisms with the same axis ratios produce different Z_{DR} and ρ_{hv}, so these habits can produce different retrieval results. The shape of particles, that is, prisms or spheroids, is an input

Corresponding author e-mail: Valery Melnikov, valery.melnikov@noaa.gov

DOI: 10.1175/JTECH-D-16-0123.1

assumption for the retrieval procedure. The retrieved parameters for these two habits are compared in section 3.

The Z_{DR} values in ice clouds are mostly positive, meaning that particles are oriented horizontally in the mean if there are no strong electric fields in clouds. Such fields are typically observed in thunderstorms. Clouds analyzed in section 3 did not produce precipitation, so measured Z_{DR} and ρ_{hv} are affected by particles' aerodynamics and cloud turbulence. The mean horizontal orientation of ice cloud particles is disturbed by their swinging and fluttering (e.g., Pruppacher and Klett 1997, section 10; Klett 1995). Such fluctuations in the orientations can be represented by a distribution in the particle's canting angle. The standard deviations in the canting angles measured in laboratories and remotely vary from 1° to more than 20° (Zikmunda and Vali 1972; Kajikawa 1976; Noel and Chepher 2004; Noel and Sassen 2005; Matrosov et al. 2005). Noel and Chepher (2004) pointed out that the orientation distributions of ice cloud particles are still unknown. The standard deviation in the distribution is one of the output parameters of the retrieval procedure (section 3). The obtained results are discussed in section 4.

2. Z_{DR} and ρ_{hv} measured with STAR radar in ice clouds

Some system parameters of a STAR radar affect the measurements of Z_{DR} and ρ_{hv}. These effects are considered in this section. The scattering of horizontally (subscript h) and vertically (subscript v) polarized electromagnetic waves is described by the scattering matrix with elements S_{mn} (m and n are any of h and v). If E_{hi} and E_{vi} are the amplitudes (positive values) and ψ_i is the differential phase of incident (subscript i) waves, then the scattered (subscript s) waves E_{hs} and E_{vs} by a single particle are written as

$$\begin{pmatrix} E_{\mathrm{hs}} \\ E_{\mathrm{vs}} \end{pmatrix} = \begin{pmatrix} S_{\mathrm{hh}} & S_{\mathrm{hv}} \\ S_{\mathrm{hv}} & S_{\mathrm{vv}} \end{pmatrix} \begin{pmatrix} E_{\mathrm{hi}} \\ E_{\mathrm{vi}} e^{j\psi_i} \end{pmatrix}, \qquad (1)$$

where j is imaginary unity. Scattered waves E_{hs} and E_{vs} are complex quantities because S_{mn} are complex, and there is phase shift ψ_i. The latter equation is written in backscatter alignment, so $S_{\mathrm{hv}} = S_{\mathrm{vh}}$. Let E_{h} and E_{v} be the amplitudes of transmitted radar waves, and then the amplitudes of incident waves can be represented as $E_{\mathrm{hi}} = \Gamma_h^{1/2} E_h$ and $E_{\mathrm{vi}} = \Gamma_{\mathrm{v}}^{1/2} E_{\mathrm{v}}$, where $\Gamma_{\mathrm{h,v}}$ are the attenuation coefficients in power units (positive and <1) at corresponding polarizations. The incident differential phase is $\psi_i = \psi_t + \Phi_{\mathrm{DP}}/2$ with Φ_{DP} being the two-way propagation differential phase and ψ_t is a differential phase acquired at transmission of the waves. The latter phase, frequently called the differential phase in transmit, is caused by radar hardware. The scattered waves travel back to radar and experience attenuation and the same propagation phase shift as the transmitted waves do, so the received waves (subscript r) can be written as $E_{\mathrm{hr}} = \Gamma_{\mathrm{h}}^{1/2} E_{\mathrm{hs}}$ and $E_{\mathrm{vr}} = \Gamma_{\mathrm{v}}^{1/2} E_{\mathrm{vs}} e^{j\psi_r + j\Phi_{\mathrm{DP}}/2}$, where ψ_r is the radar differential phase in receive. The latter phase is caused by the different signal paths in radar hardware and differs from ψ_t because the signal paths in transmit and in receive are different.

The amplitudes of transmitted waves in a STAR radar are generally different. Gains in the receive channels can be different also. So, a STAR radar is characterized with a system Z_{DR} bias and a measurement of this bias is called Z_{DR} calibration. To calibrate Z_{DR} with an external target, measurements of the reflected powers from a metal sphere (e.g., Bringi and Chandrasekar 2001, section 6.3; Williams et al. 2013), light rain, and Bragg scatter from clear air (Cunningham et al. 2013; Ice et al. 2014) have been used. These methods measure coefficient β such that for a target with intrinsic Z_{DR} of 0 dB (e.g., metal sphere, drizzle, or clear air), the received powers are related as follows: $P_{\mathrm{vr}} = \beta P_{\mathrm{hr}}$, where β is the system Z_{DR}. Let β_t and β_r be the transmitter's and receiver's contributions, respectively, to the system Z_{DR}; that is $E_{\mathrm{v}} = \beta_t E_{\mathrm{h}}$ and $E_{\mathrm{vr}} = \beta_r E_{\mathrm{hr}}$. Then $\beta = (\beta_r \beta_t)^2$ for a target with an intrinsic Z_{DR} value of 0 dB. Differential gains β_t and β_r are different because the transmit and receive signal paths are different. Differential gains β_t and β_r are sometimes called transmitter's and receiver's biases, respectively (e.g., Cunningham et al. 2013; Ice et al. 2014). The received waves can be written as

$$\begin{pmatrix} E_{\mathrm{hr}} \\ E_{\mathrm{vr}} \end{pmatrix} = C_R \begin{pmatrix} \Gamma_{\mathrm{h}}^{1/2} & 0 \\ 0 & \Gamma_{\mathrm{v}}^{1/2} \beta_r e^{j\psi_r + j\Phi_{\mathrm{DP}}/2} \end{pmatrix} \begin{pmatrix} S_{\mathrm{hh}} & S_{\mathrm{hv}} \\ S_{\mathrm{hv}} & S_{\mathrm{vv}} \end{pmatrix} \times \begin{pmatrix} \Gamma_{\mathrm{h}}^{1/2} & 0 \\ 0 & \Gamma_{\mathrm{v}}^{1/2} e^{j\psi_t + j\Phi_{\mathrm{DP}}/2} \end{pmatrix} \begin{pmatrix} E_{\mathrm{h}} \\ \beta_t E_{\mathrm{h}} \end{pmatrix}, \qquad (2)$$

where C_R is the radar constant with range normalization and the range phase is included. This constant and the amplitude E_{h} will be omitted in the following discussion without any loss of generality because Z_{DR} and ρ_{hv} are relative quantities and do not depend on these parameters. The transmission matrixes in (2) are written in a diagonal form, which means that depolarization in the propagation media is neglected. Equation (2) can be represented as

$$E_{\mathrm{hr}} = \Gamma_{\mathrm{h}} S_{\mathrm{hh}} + (\Gamma_{\mathrm{h}}\Gamma_{\mathrm{v}})^{1/2} \beta_t S_{\mathrm{hv}} e^{j\psi_t + j\Phi_{\mathrm{DP}}/2} \quad \text{and} \qquad (3)$$

$$E_{\mathrm{vr}} = [\Gamma_{\mathrm{v}} \beta_t S_{\mathrm{vv}} e^{j\psi_t + j\Phi_{\mathrm{DP}}/2} + (\Gamma_{\mathrm{h}}\Gamma_{\mathrm{v}})^{1/2} S_{\mathrm{hv}}] \beta_r e^{j\psi_r + j\Phi_{\mathrm{DP}}/2}. \qquad (4)$$

Platelike and columnar particles are characterized with two polarizabilities α_{h} and α_{v} along the major and minor axes, where α_h refers to the longer axis. In the Rayleigh scattering limit, the scattering matrix for a single scatterer can be represented as

$$S_{hh} = \alpha_h + \Delta\alpha \sin^2\theta \sin^2\varphi, \quad S_{vv} = \alpha_h + \Delta\alpha B^2,$$
$$S_{hv} = \Delta\alpha B \sin\theta \sin\varphi, \tag{5}$$
$$\Delta\alpha = \alpha_v - \alpha_h, \quad \text{and}$$
$$B = \sin\gamma \sin\theta \cos\varphi + \cos\gamma \cos\theta, \tag{6}$$

where θ is the canting angle of the scatterer in the laboratory frame, φ is the orientation angle on the horizontal plane, and γ is the elevation angle of a radar antenna [e.g., Bringi and Chandrasekar 2001, (2.53)]. The laboratory frame is a coordinate system affixed to the ground; that is, the plane XOY is horizontal and the O–Z axis is vertical. Scattering geometry can also be represented in the scattering plane (e.g., Holt 1984; Vivekanandan et al. 1991; Ryzhkov and Zrnić 2007). The laboratory frame is used in this study because it is natural for representing canting of atmospheric particles: angle θ is the canting angle in the laboratory frame by definition. This angle is used in laboratory measurements of particles' orientation (e.g., Zikmunda and Vali 1972; Kajikawa 1976) and in lidar remote sensing techniques (e.g., Noel and Sassen 2005; Platt 1978; Platt et al. 1978).

The depolarized waves are described by the addends in (3) and (4) containing $S_{hv} \sim \Delta\alpha$. In ice clouds at large Z_{DR}, $|\alpha_v|$ is much smaller than $|\alpha_h|$, thus $|\Delta\alpha| \sim |\alpha_h|$, and the amplitudes of the depolarized waves are comparable with the amplitudes of the primary backscattered waves. So, depolarization can substantially contribute to Z_{DR} and ρ_{hv} measured by a STAR radar in ice clouds.

Substitution of (5) into (3) and (4) yields

$$E_{hr} = \alpha_h \Gamma_h + \Delta\alpha \Gamma_h^{1/2} A \sin\theta \sin\varphi, \tag{7}$$
$$E_{vr} = (\alpha_h \Gamma_v \beta_t e^{j\psi_t + j\Phi_{DP}/2} + \Delta\alpha \Gamma_v^{1/2} AB)\beta_r e^{j\psi_r + j\Phi_{DP}/2}, \tag{8}$$

with

$$A = \Gamma_h^{1/2} \sin\theta \sin\varphi + \Gamma_v^{1/2} B \beta_t e^{j\psi_t + j\Phi_{DP}/2}. \tag{9}$$

Data analyzed in the next section were collected with the S-band WSR-88D. For S-band radiation propagating in ice clouds, the propagation differential phase shift and differential attenuation are frequently negligible—that is, $\Gamma_{h,v} \approx 1$ and $\Phi_{DP} \approx 0$ and (7) and (8) are simplified to

$$E_{hr} = \alpha_h + \Delta\alpha A_o \sin\theta \sin\varphi, \tag{10}$$
$$E_{vr} = \beta_r e^{j\psi_r}(\alpha_h \beta_t e^{j\psi_t} + \Delta\alpha A_o B), \quad \text{and} \tag{11}$$
$$A_o = \sin\theta \sin\varphi + B\beta_t e^{j\psi_t}. \tag{12}$$

Equations (10) and (11) are valid for arbitrary orientations of scatterers; they can be applied for hydrometeors having nonzero mean canting angles. In the absence of strong electric fields in clouds, ice hydrometeors fall downward with their largest axis being horizontal in the mean (Pruppacher and Klett 1997, chapter 10), so the mean canting angle is zero. Radar data analyzed in the next section were collected in nonprecipitating clouds; thus, a mean canting angle of zero is assumed. The rest of this section is valid for the zero mean canting angle.

The radar volume contains many scatterers that change their orientations over time. The radar variables are obtained by time averaging of the products of amplitudes E_{hr} and E_{vr}. Because of ergodicidy, time averaging is equivalent to spatial and orientation averaging. The latter can be done by introducing probability $P(\theta, \varphi)\sin\theta d\theta d\varphi$ to have the orientation angles in intervals from θ to $\theta + d\theta$ and from φ to $\varphi + d\varphi$. Assuming that the orientation angles and particle sizes are independent, averaging over orientations and sizes can be separated. This assumption does not limit the obtained results because all radar-measured parameters are some mean values obtained by averaging over all particles in the radar resolution volume.

In the orientation averaging, θ and φ distributions are assumed to be independent. Distributions over φ can be considered uniform because fluttering and swinging of cloud particles randomize orientations on the horizontal plane. For the uniform φ distribution, $\langle\sin\varphi\rangle = \langle\sin^3\varphi\rangle = 0$, $\langle\sin^2\varphi\rangle = 1/2$, $\langle\sin^4\varphi\rangle = 3/8$, and $\langle\sin^2\varphi \cos^2\varphi\rangle = 1/8$, where the angular brackets stand for orientation averaging.

The mean received powers P_h and P_v in the polarization channels are obtained as

$$P_h = \langle|E_{hr}|^2\rangle \quad \text{and} \quad P_v = \langle|E_{vr}|^2\rangle. \tag{13}$$

Values of Z_{DR} and ρ_{hv} are

$$Z_{DR} = 10\log_{10}[(P_h - n_h)/(P_v - n_v)], \tag{14}$$
$$R_{hv} = \langle E_{hr}^* E_{vr}\rangle, \quad \text{and} \tag{15}$$
$$\rho_{hv} = |R_{hv}|/[(P_h - n_h)(P_v - n_v)]^{1/2}, \tag{16}$$

where n_h and n_v are the mean noise powers in the channels. Averaging in (13) and (15) yields

$$P_h = \langle|\alpha_h|^2\rangle + J_1 \mathrm{Re}(\langle\alpha_h^* \Delta\alpha\rangle) + \langle|\Delta\alpha|^2\rangle C_1, \tag{17}$$
$$P_v = \beta_r^2[\langle|\alpha_h|^2\rangle\beta_t^2 + 2\mathrm{Re}(\langle\alpha_h^*\Delta\alpha\rangle)\beta_t^2 C_2 + \langle|\Delta\alpha|^2\rangle C_3], \tag{18}$$

$$R_{\mathrm{hv}} = \beta_r\beta_t e^{j\psi_{sys}}[\langle|\alpha_{\mathrm{h}}|^2\rangle + \mathrm{Re}(\langle\alpha_h\Delta\alpha^*\rangle)C_4 + j\mathrm{Im}(\langle\alpha_h\Delta\alpha^*\rangle)C_5 + \langle|\Delta\alpha|^2\rangle C_6], \quad (19)$$

$$C_1 = [3J_2 + 4(J_1 - J_2)\beta_t^2 + (5J_2 - 4J_1)\beta_t^2\sin^2\gamma]/8, \quad (20a)$$

$$C_2 = 1 - J_1 - (1 - 3J_1/2)\sin^2\gamma, \quad (20b)$$

$$C_3 = (J_1 - J_2)/2 + \beta_t^2(1 - 2J_1 + J_2) + [(5J_2 - 4J_1)/8 - \beta_t^2(2 - 7J_1 + 5J_2)]\sin^2\gamma + \beta_t^2(1 - 5J_1 + 35J_2/8)\sin^4\gamma, \quad (20c)$$

$$C_4 = 1 - J_1/2 + (3J_1/2 - 1)\sin^2\gamma, \quad (20d)$$

$$C_5 = (1 - 3J_1/2)\cos^2\gamma, \quad (20e)$$

$$C_6 = e^{-j\psi_t}\cos\psi_t[J_1 - J_2 + (5J_2/4 - J_1)\sin^2\gamma], \quad \text{and} \quad (20f)$$

$$\psi_{\mathrm{sys}} = \psi_t + \psi_r, \quad (20g)$$

where Re(x) and Im(x) stand for the real and imaginary parts of x, respectively, and

$$J_1 = \langle\sin^2\theta\rangle, \quad J_2 = \langle\sin^4\theta\rangle \quad (21)$$

are the moments of the θ distribution (see the appendix). Measurables (14) and (16) of a STAR radar are explicitly expressed via polarizabilities, moments (21) of the θ distribution, elevation angle γ, system biases $\beta_{t,r}$, and differential phases in transmit and receive $\psi_{t,r}$. The elevation dependences of Z_{DR} and ρ_{hv} were obtained by Myagkov et al. (2016) for the radar system phases of zero and equal channel gains. One can see from (17) to (19) that depolarization of radar waves affects Z_{DR} and ρ_{hv} measured with STAR radar. These effects were studied by Ryzhkov and Zrnić (2007) and Hubbert et al. (2014a,b).

Equation (18) shows that to obtain correct Z_{DR} measured by a STAR radar, system biases β_t and β_r should be known. This is in contrast to radar with alternate polarizations, for which product $\beta_t^2\beta_r^2$ is the system Z_{DR} bias. For a STAR radar, the system biases enter in P_{v} in a more complicated form. If a scattering media has small intrinsic Z_{DR}—for instance, drizzle—then $|\Delta\alpha| \ll |\alpha_{\mathrm{h}}|$ and (17) and (18) reduce to $P_{\mathrm{h}} = \langle|\alpha_{\mathrm{h}}|^2\rangle$ and $P_{\mathrm{v}} = \beta_r^2\beta_t^2[\langle|\alpha_{\mathrm{h}}|^2\rangle$, so Z_{dr} in power units is $\beta_r^2\beta_t^2$, which is system Z_{dr}. The latter shows that the product of biases is sufficient for Z_{DR} calibration of a STAR radar in such a case as it is for a radar with alternate polarizations. In ice clouds $|\Delta\alpha|$ can be comparable with $|\alpha_{\mathrm{h}}|$ and P_{v} has form (18), so β_t and β_r should be separately measured in a STAR radar and taken into consideration in the retrieval procedure (see section 3a).

It follows from (17) and (18) that P_{h}, P_{v}, respectively, and Z_{DR} do not depend upon the system differential phase ψ_{sys}. This is a consequence of the uniform φ distribution and a mean canting angle of zero. If one (or both) of these conditions is (are) not satisfied, then ψ_{sys} affects the powers and Z_{DR}. Equation (19) shows that ψ_t affects the modulus of R_{hv} even at the uniform φ distribution.

3. Retrieval of the ice particles' parameters

a. Overview of the retrieval procedure

Let a and b be the major and minor axes, respectively, of a platelike ice particle. The retrieval procedure aims at obtaining the axis ratio a/b and the degree of orientation σ_θ from measured Z_{DR} and ρ_{hv}. The degree of orientation σ_θ is the standard deviation in the canting angle θ, that is, $\sigma_\theta = \langle\theta^2\rangle^{1/2}$ [see also (A4) in the appendix]. The Gaussian and Fisher distributions in orientations are used frequently (e.g., Matrosov et al. 2005; Hubbert et al. 2014a). The Gaussian distribution has been used in this study, and it is shown in the appendix that moments J_1 and J_2, which enter into (17)–(19), and (21), are about the same for the Gaussian and Fisher distributions.

Equations (14) and (16) connect measured Z_{DR} and ρ_{hv} with a/b and σ_θ through (17)–(19). Equation (14) does not distinctively have the system Z_{DR} addend. System biases β_t and β_r enter into (17)–(19) in a more complicated way than their product. So, to create a lookup table that connects a/b and σ_θ with measured Z_{DR} and ρ_{hv}, (14) and (16) have been used for input arrays of a/b and σ_θ using measured β_t and β_r. The input arrays contain a/b and σ_θ in the following intervals: $1 \le a/b \le 50$ (stride = 0.1) and $1° \le \sigma_\theta \le 90°$ (stride = 1°). The Z_{DR} and ρ_{hv} have been calculated using these input arrays at each elevation angle from 0° to 60°, that is, to the maximum WSR-88D's elevation angle. So, the lookup table is a 3D matrix (61, 500, 90), that is, (#elevation angles, #a/b, #σ_θ).

To create the lookup table for the KOUN radar (Norman, Oklahoma), biases β_t and β_r should be obtained. Parameter β_r experiences weak variations over time caused by instabilities of receivers' gains; it is measured using solar radiation. The sun is a source of unpolarized radiation, so a Z_{DR} value from it is 0 dB. Parameter β_r equals a Z_{DR} value measured at the center of the sun. In KOUN it was 0.23 dB in case 1, that is, 1.054 in power units; in case 2 it was 0.30 dB, that is, 1.072 in power units (see the cases below). To obtain β_t, Bragg scatter observations have been utilized. Bragg scatter has an intrinsic Z_{DR} value of 0 dB, so the mean Z_{DR} value from Bragg scatter equals to β. In case 1 it was 0.22 dB, that is, 1.052 in power units; in case 2 it was

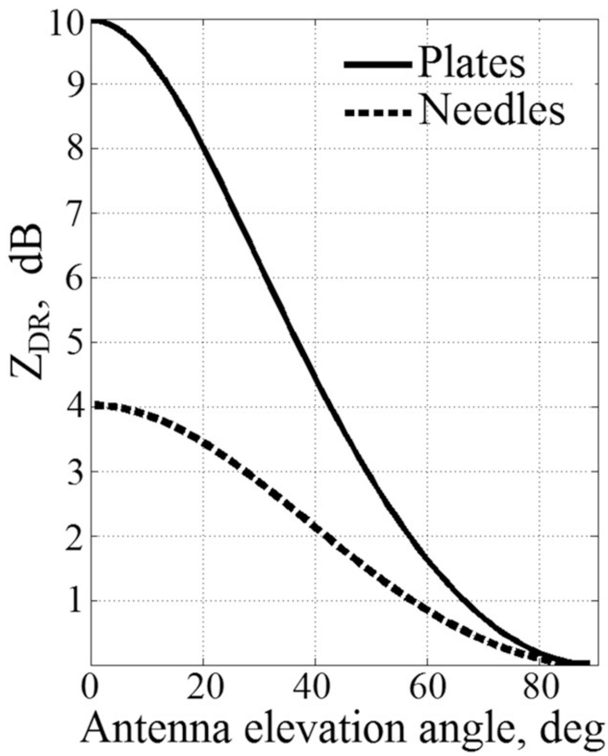

FIG. 1. Radar differential reflectivity Z_{DR} as a function of the antenna elevation angle for very thin horizontally oriented ice plates (solid line) and needles (dash line).

0.29 dB, that is, 1.069 in power units. Parameter β_t has been obtained from $\beta = (\beta_r\beta_t)^2$: it was $\beta_t = 0.97$ and 0.96 in cases 1 and 2, respectively.

If measured Z_{DR} exceeds 4 dB, then ice scatterers have platelike shapes (Hogan et al. 2002; Melnikov and Straka 2013). Such Z_{DR} values are typically observed at low antenna elevation angles. Values of Z_{DR} decrease with the elevation angle. Figure 1 depicts elevation angle dependences of Z_{DR} for very thin ice plates and needles ($a/b > 50$) oriented strictly horizontally ($\sigma_\theta = 0°$). To apply the retrieval procedure, the shape factors $L_{h,v}$ [see (22) below] should be determined. These factors are different for ice plates and needles. Distinguishing between platelike and columnar (needles) ice particles can be done by using measured Z_{DR}. One can see from Fig. 1 that if Z_{DR} is larger than 4 dB at low elevations, then the scatterers have platelike shapes. At an elevation of, for instance, 40°, this threshold is 2 dB. So, cloud areas with platelike particles producing $Z_{DR} > 4$ dB at low elevation angles (category B from Williams et al. 2015) are analyzed in this study.

The curves in Fig. 1 have been generated for pristine ice plates and needles. Ice particles of more complicated habits can be characterized with bulk density that is obtained as a volume fraction of ice in a particle. Bulk density can be much lower than density of solid ice. Cloud particles having lager σ_θ or/and lower bulk density have lower Z_{DR} values. So, if measured Z_{DR} values are larger than those shown with the dash curve in Fig. 1, then the particles have platelike shapes. This curve has been used to identify areas filled with platelike ice particles at all available elevation angles.

At S frequency band, cloud ice particles are much smaller than the radar wavelength, which is nearly 10 cm. So, such particles are Rayleigh scatterers, and parameters α_h and α_v in (17)–(19) depend on the shape of a scatterer as

$$\alpha_{h,v} = V\frac{\varepsilon - 1}{L_{h,v}(\varepsilon - 1) + 1}, \tag{22}$$

where $L_{h,v}$ are the shape factors, V is the volume of the scatterer, and ε is its dielectric permittivity. Shape factors $L_{h,v}$ for spheroids can be found, for instance, in Bringi and Chandrasekar (2001, section A1.1). The shapes of platelike particles are close to hexagonal prisms for which $L_{h,v}$ were obtained by Westbrook (2014). For very thin plates and needles, α_h and α_v for spheroids and prisms are the same at equal axis ratios. So the rule for distinguishing plates and needles (Fig. 1) is the same for spheroids and prisms.

A choice between prisms and spheroids is an input assumption for the retrieval procedure. The shapes of real pristine ice particles are close to prisms, so the retrieval results for prisms are considered herein to be more representative values than those for spheroids. The retrieval results for spheroids are shown below as well for comparisons.

The measured Z_{DR} and ρ_{hv} values are estimates, so the retrieved a/b and σ_θ values have some uncertainties, which depend upon the radar dwell time, the signal-to-noise ratio (SNR), the spectrum width, and the intrinsic correlation coefficient (Melnikov and Zrnić 2007). Such uncertainties are sometimes called statistical errors because they originate from natural fluctuations of the estimates. These errors can be reduced by either increasing the measurement dwell time or signal processing (for instance, by applying the spectral analysis to increase SNR). The statistical uncertainties in Z_{DR} and ρ_{hv} measurements have been obtained using their standard deviations ΔZ_{DR} and $\Delta\rho_{hv}$, so true Z_{DR} and ρ_{hv} lie in the intervals from $Z_{DR} - \Delta Z_{DR}$ to $Z_{DR} + \Delta Z_{DR}$ and from $\rho_{hv} - \Delta\rho_{hv}$ to $\rho_{hv} + \Delta\rho_{hv}$; that is, the 1σ uncertainties have been utilized. To obtain the statistical uncertainties in a/b and σ_θ, eight pairs of Z_{DR} and ρ_{hv} (Z_{DR}, $\rho_{hv} - \Delta\rho_{hv}$; Z_{DR}, $\rho_{hv} + \Delta\rho_{hv}$; $Z_{DR} - \Delta Z_{DR}$, ρ_{hv}; $Z_{DR} + \Delta Z_{DR}$, ρ_{hv}; $Z_{DR} - \Delta Z_{DR}$, $\rho_{hv} - \Delta\rho_{hv}$; $Z_{DR} - \Delta Z_{DR}$, $\rho_{hv} + \Delta\rho_{hv}$; $Z_{DR} + \Delta Z_{DR}$, $\rho_{hv} - \Delta\rho_{hv}$; $Z_{DR} + \Delta Z_{DR}$, $\rho_{hv} + \Delta\rho_{hv}$) have been used to

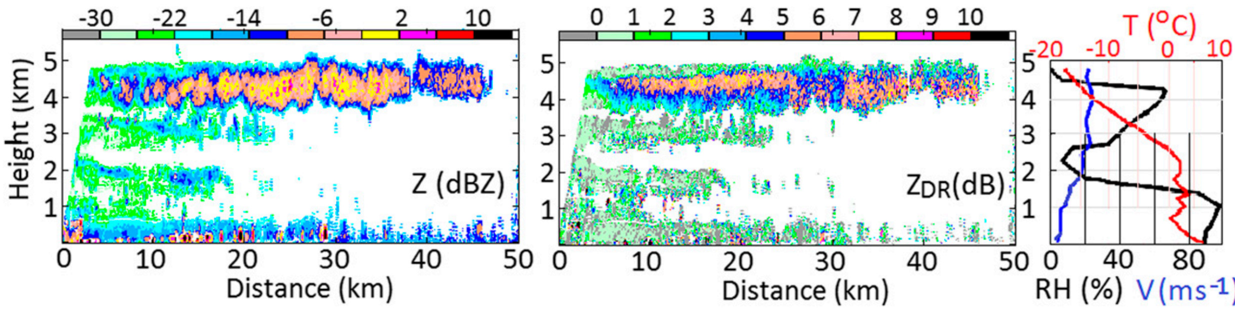

FIG. 2. Vertical cross sections of (left) reflectivity and (center) differential reflectivity at 1855 UTC 23 Mar 2013 at an azimuth of 270°. (right) The rawinsonde data collected at the KOUN site at 0000 UTC 24 Mar 2013; T is the temperature (red curve), RH is relative humidity (black curve), and V is the horizontal wind velocity (blue line).

retrieve eight pairs of a/b and σ_θ from which the maximal uncertainties $\Delta(b/a)$ and $\Delta(\sigma_\theta)$ have been taken.

b. Case 1: 23 March 2013

An example of layered nonprecipitating clouds observed with the S-band WSR-88D KOUN radar is shown in Fig. 2. One can see a layer of $Z_{DR} > 4$ dB at heights around 4.5 km (the center panel). For such Z_{DR}, cloud particles have platelike shapes. There are three more layered echoes below this cloud, but our focus is on the clouds located above 3.5 km.

Figure 3a displays the radar echo shown with gray and areas occupied by platelike particles shown with red. The red areas have been obtained by utilizing the dependences shown in Fig. 1. One can see in Figure 3a that almost the entire cloud contains platelike ice particles. The cloud areas, where the retrieval of a/b has not been conducted, are gray. In these areas, platelike particles have not been identified by utilizing the curves in Fig. 1, but this does not mean that the areas do not contain ice plates. It means that the particles' axis ratios are not large enough to be unambiguously identified as plates. So, the retrieval has not been conducted in the gray areas. The temperatures at heights of 3.5–4.5 km were in an interval from −8° to −17°C (Fig. 2, right panel), which is favorable for growing platelike ice crystals (Bailey and Hallet 2009).

Figure 3b shows a field of the retrieved a/b. This field is smaller than the field of platelike particles in Fig. 3a because in some radar range gates, the SNR is weaker than 10 dB and the ρ_{hv} values are lower than the minimal possible ones, that is, 0.898 (the appendix). The latter issue is caused by 1) natural fluctuations in the estimates and 2) contaminations from ground clutter. The quality of ρ_{hv} estimates is characterized by its standard deviation, which depends on the SNR, spectrum width, intrinsic ρ_{hv}, and dwell time (e.g., Bringi and Chandrasekar 2001, section 6.5; Melnikov and Zrnić 2007). The estimate can deviate from the true ρ_{hv} value, and some negative deviations can make the estimate smaller than 0.898. Cause 2 is due to not fully suppressed ground clutter leaking through the antenna sidelobes. The radar data have been processed with a ground clutter filter on, but at some azimuths, ground clutter is so strong that it cannot be completely suppressed by the filter. Such contaminations are noticeable within distances of about 10–12 km from the radar. In a range gate having ρ_{hv} smaller than 0.898, the retrieval has not been conducted and the range gate has been painted with gray in the panel. One can see a pattern in the a/b field: the axis ratios decrease with decreasing height, which could be due to the growth processes.

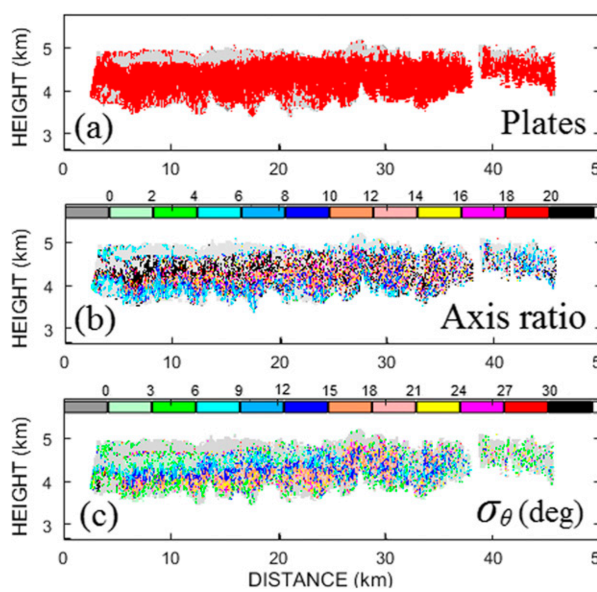

FIG. 3. (a) Cloud areas occupied by platelike ice particles are shown with red. The rest of the radar echo is painted with light gray. (b) Axis ratios a/b in the areas of platelike particles in the shape of a prism. (c) The degree of orientation σ_θ in areas of platelike ice particles of the prism shapes. The gray color in (b) and (c) shows areas where the retrieval has not been conducted.

Figure 3c shows a field of σ_θ. A decrease in σ_θ with height is apparent. This pattern could be due to the following factors: 1) Dynamic processes in the cloud bottom are more intense than those in the cloud top. 2) Ice particles with larger a/b could be more stable in the air than those with lower a/b. One can see a correlation between areas occupied by the particles with larger a/b and areas with lower σ_θ. The wind shears and small-scale turbulence affect orientations of cloud particles. At the same turbulence intensity, the particles with smaller a/b could experience more intense flutter than those having larger a/b.

The shapes of pristine ice cloud particles are closer to prisms than to spheroids. To obtain a dependence of the retrieved parameters on these shapes, the statistical uncertainty of the retrieval has been targeted to a value of about 40%. For such a value, the SNR of radar returns should be stronger than 10 dB. Figure 4 presents scatterplots of a/b and σ_θ for prisms and spheroids in radar range gates where SNR > 10 dB and $\rho_{hv} > 0.898$. The median a/b values for prisms and spheroids are 14 and 9, respectively. The results reveal the presence of very thin ice particles with $a/b > 10$: 57% (30%) of the values for prisms (spheroids) have such axis ratios. The retrieved values of σ_θ are nearly the same for both habits; the median value of σ_θ is 12°, which corresponds to the moderate degree of orientation.

The number of measurements in Fig. 4 is 1403, from which 363 measurements have $\Delta(a/b)$ or $\Delta(\sigma_\theta)$ larger than 100%. The analysis shows that data with $\Delta(a/b) >$ 100% have $a/b > 50$; that is, the particles have extremely large axis ratios. The data with $\Delta(\sigma_\theta) > 100\%$ have σ_θ values in an interval of 1°–2°; that is, the particles are oriented almost horizontally. Figure 5 presents a scatterplot of $\Delta(a/b)$ and $\Delta(\sigma_\theta)$ in percent for the pairs having $\Delta(b/a)$ and $\Delta(\sigma_\theta) < 100\%$. The median statistical errors in a/b and σ_θ are 38% and 26%, respectively, which are acceptable statistical uncertainties because the maximal 1σ errors have been chosen.

Noisiness in the a/b and σ_θ fields is evident. It could be partially due to natural variability in the axis ratios and orientations, and it could be caused by the uncertainties in the retrieved parameters introduced by fluctuations of the measured Z_{DR} and ρ_{hv} values. The mean statistical uncertainties are 38% and 26% for a/b and σ_θ, but some measurements have these errors as large as 90%. Such errors contribute to the noisiness of the fields.

c. *Case 2: 15 August 2016*

Vertical cross sections of another case (Fig. 6) exhibit a patchier reflectivity field and a more complicated Z_{DR} field than those in case 1. The echoes below

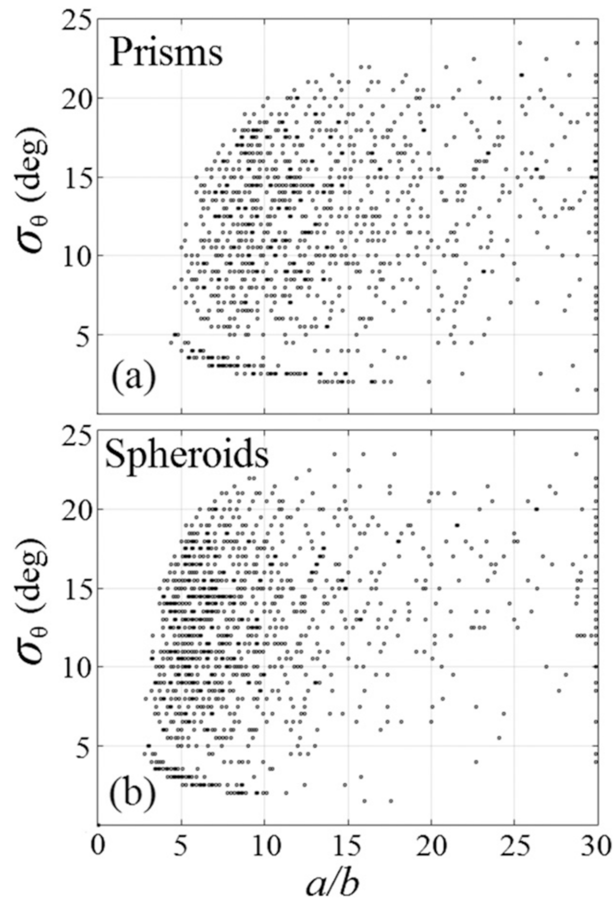

FIG. 4. The retrieved axis ratios and degrees of orientation for (a) prisms and (b) spheroids obtained for the areas of the platelike particles (Fig. 3a) and SNR > 10 dB.

3 km are from atmospheric biota and have not been analyzed. Figure 7a exhibits areas occupied by platelike particles obtained with the diagram in Fig. 1. The fields in Figs. 7b and 7c have been obtained similarly to those shown in Fig. 3. There are compact areas of certain retrieved values in Figs. 7b and 7c, but their patterns are more complicated than those in Fig. 3. This is most likely due to a more complicated wind field in the cloud. The temperatures at heights of 5.5–7.5 km were in an interval from −10° to −18°C (Fig. 6, right panel), which is favorable for growing platelike ice crystals.

Figure 8 presents scatterplots of the axis ratios and the degree of orientation assuming the prismatic (Fig. 8a) and spheroidal (Fig. 8b) shapes of particles. The mean axis ratios for prisms and spheroids are 16 and 13, respectively. The degree of orientations is 17° for both habits, which points to sufficiently strong dynamic processes in the cloud. Figure 9 presents statistical uncertainties in the retrieved a/b and σ_θ for prisms. The median $\Delta(a/b)$ is 43% and the median $\Delta(\sigma_\theta)$ is 18%.

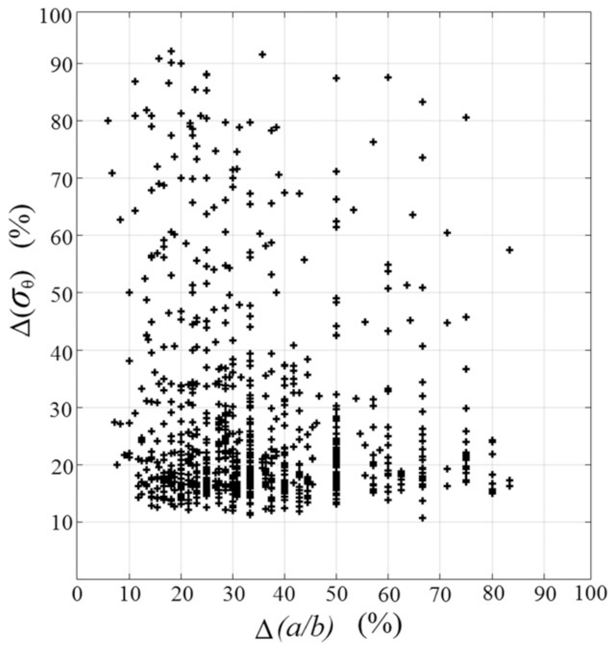

FIG. 5. The 1σ statistical uncertainties in the retrieved a/b and σ_θ for the results in Fig. 4 for prisms.

4. Discussion and conclusions

Equations (7) and (8) for the amplitudes of backscattered waves received by a STAR (simultaneous transmission and reception of polarized waves) radar are derived in terms of particles' polarizabilities, the propagation phase, radar system phases, channel differential gains in transmit and receive, the orientation of particles, and the antenna elevation angle. Equations (17)–(19) are obtained for a mean canting angle of 0° for hydrometeors in stratiform clouds.

The median axis ratios of cloud platelike ice particles (a/b, where a and b are their major and minor axes, respectively) and the standard deviation in their canting angles (σ_θ) have been retrieved from measured radar differential reflectivity (Z_{DR}) and correlation coefficient (ρ_{hv}) using (14) and (16), respectively. If the measured Z_{DR} exceeds the value obtained for a prolate scatterer (the dash curve in Fig. 1), then the scatterers have platelike shapes. This approach has been used to obtain areas containing platelike particles (Figs. 3a and 7a). Figure 1 has been generated for pristine ice plates and columns. If ice particles are characterized with bulk density that is lower than the density of solid ice, then their Z_{DR} values are smaller than those obtained for pristine ice plates. Thus, the approach of identifying ice plates remains correct for particles of bulk density, but the obtained cloud areas, containing the plates, could be smaller than the actual ones. This approach can be used in the operational WSR-88Ds to obtain cloud areas filled with platelike particles.

To retrieve a/b and σ_θ, the system differential phase in transmit (ψ_t) and differential gains (β_t and β_r) in the polarization channels must be known. The system differential phase in receive (ψ_r) does not affect measured Z_{DR} and ρ_{hv} in stratiform clouds, where particles have a mean canting angle of zero.

Ice cloud particles are characterized with distributions in sizes and orientations. The retrieval procedure utilizes the Z_{DR} and ρ_{hv} values averaged over these distributions. So, the retrieved a/b and σ_θ should be considered as the mean values averaged over the same distributions.

The measured Z_{DR} and ρ_{hv} are estimates in the statistical sense due to natural fluctuations of radar returns. The median statistical uncertainties in the retrieved a/b and σ_θ are 40% and 20%, respectively, in the analyzed cases. These uncertainties have been obtained by throwing away about 9% of the measurements that had

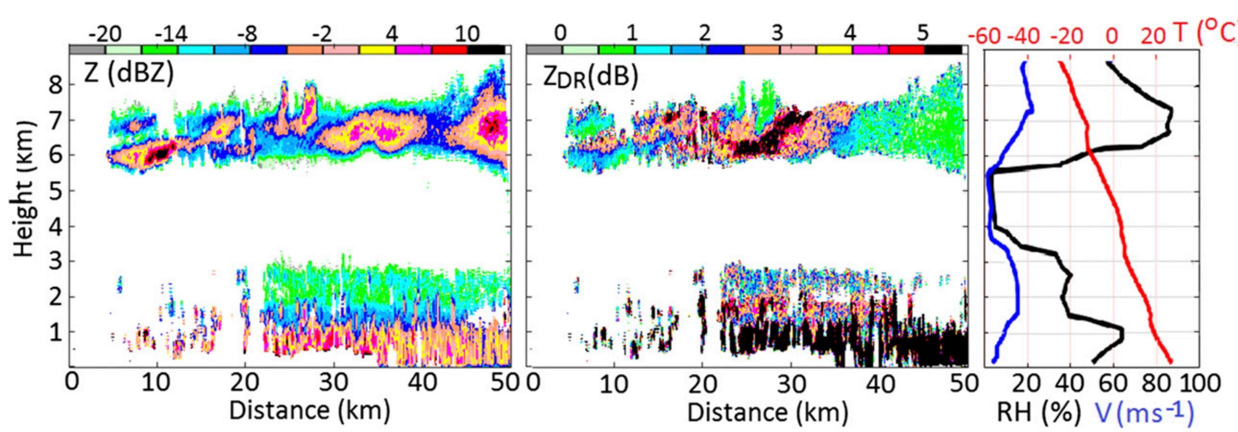

FIG. 6. As in Fig. 2, but at 0049 UTC 15 Aug 2016 at an azimuth of 40°. The rawinsonde data were collected at the KOUN site at 0000 UTC on the same day.

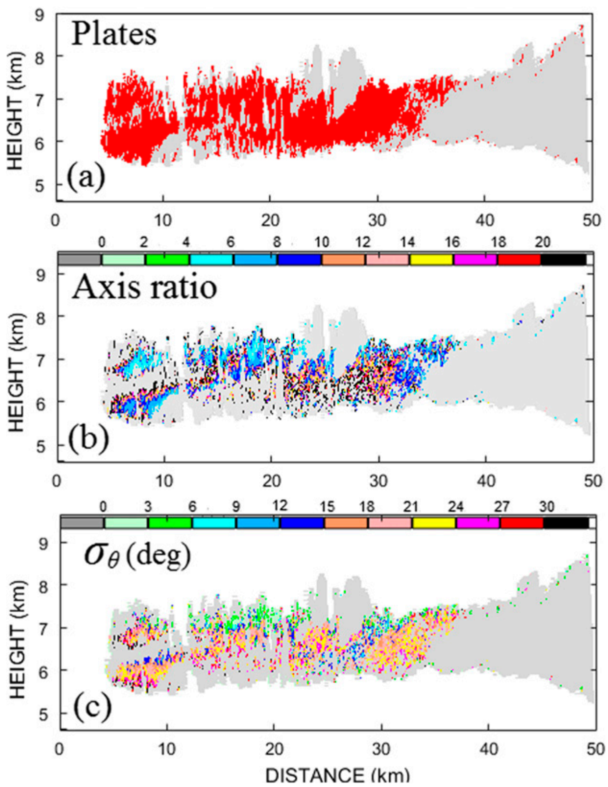

FIG. 7. As in Fig. 3, but for case 2.

statistical errors larger than 100%. In such measurements, the retrieved a/b values are larger than 50 or $\sigma_\theta \leq 2°$; that is, the particles were extremely thin or oriented strictly horizontally.

The retrieved a/b values depend on the assumed shapes of ice plates, that is, prisms or spheroids. The retrieved median a/b are 14 and 16 in cases 1 and 2, respectively, assuming the prism shape of the particles; that is, the particles are thin. Thin particles have been observed in stratiform clouds with lidars (e.g., Platt 1977, 1978; Platt et al. 1978; Westbrook et al. 2010) that indicate that cloud ice particles have a prism habit rather than the spheroidal shape because specular reflection from spheroids is much weaker than that from prisms (Mishchenko et al. 1997). Spheroids are frequently used in scattering problems; therefore, the retrieval results for prisms and spheroids have been compared. The retrieved axis ratios for prisms and spheroids (Figs. 4 and 8) are noticeably different. The median a/b values for prisms is 14 (16), whereas for spheroids it is 9 (13) in case 1 (case 2). An ice prism has more ice at its edges than a spheroid does. Therefore, at the same axis ratio, a spheroid is more oblate than a prism and produces larger Z_{DR} than that from a prism. Thus, at the same Z_{DR}, a retrieved a/b for a prism is larger than that for a spheroid. Since prisms are better approximations for real cloud ice particles, the retrieved a/b for prisms are considered here to be more representative values than those for spheroids.

The retrieved σ_θ values (Figs. 4 and 8) span a wide interval from 2° to 23° and are nearly the same for the prisms and spheroids. The median values of σ_θ are 12° in case 1 and 17° in case 2, which correspond to a moderate degree of orientation. These values are close to those measured by Garrett et al. (2015) in snow. Matrosov et al. (2005) obtained σ_θ in ice clouds in an interval from 3° to 15°. Photographic laboratory measurements by Kajikawa (1976) indicated canting of 10°–25°. Zikmunda and Vali (1972) measured mean canting of rimed crystals in an interval of 5°–15°, but a few crystals exhibited canting of 75°. Melnikov and Straka (2013) obtained σ_θ in an interval from 2° to 20°. The wide σ_θ span discussed in section 3 points to sufficiently strong dynamic processes in the analyzed clouds. The KOUN radar's data archive shows that clouds having areas with $Z_{\mathrm{DR}} > 4$ dB—that is, having platelike particles—are typically not homogeneous and form "pockets" of high Z_{DR} values

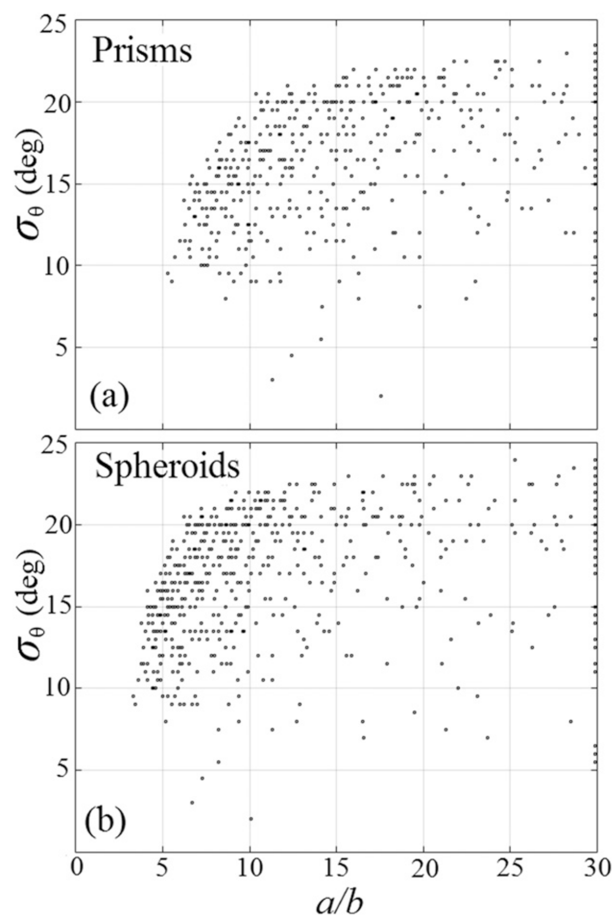

FIG. 8. As in Fig. 4, but for case 2.

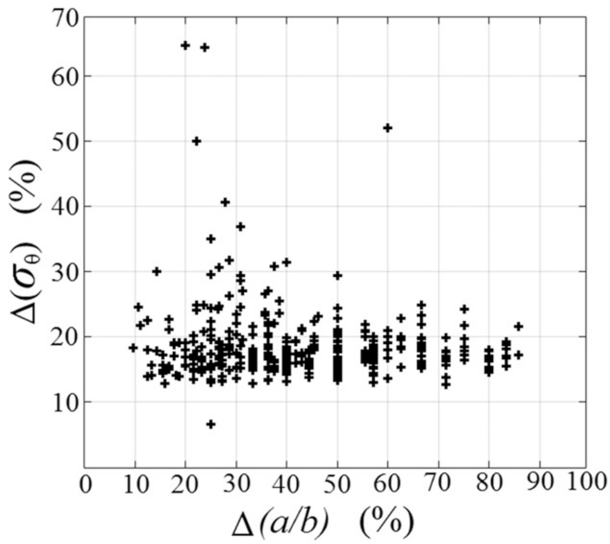

FIG. 9. As in Fig. 5, but for case 2.

surrounded by areas of much lower Z_{DR} (e.g., Melnikov et al. 2011). The spotty reflectivity fields (the left panels in Figs. 2 and 6) also point to sufficiently strong dynamic processes in the analyzed clouds.

Ice particles in shapes of plate prisms and spheroids have been considered in this study. Particles of more complicated shapes (for instance, dendrites) can also be approximated with fitted prisms or spheroids (e.g., Tyynelä et al. 2011; Hogan et al. 2012; Matrosov 2015). Such particles are considered as a mixture of ice and air. This approach allows for introducing bulk ice density, which can be much smaller than density of solid ice. Note that Z_{DR} from a particle of bulk density is smaller than that of solid ice at the same axis ratio. The retrieval procedure produces a larger retrieved a/b for particles with bulk ice density than that for particles of solid ice (Melnikov and Straka 2013). So, the retrieved axis ratios obtained for solid ice particles can be considered as the estimation from below for particles having bulk ice density. The median $a/b = 14$ (case 1) and 16 (case 2) obtained for prisms should be considered as the minimal axis ratios in the analyzed clouds, and the actual a/b can be larger for particles having bulk ice density. Despite this retrieval uncertainty, the estimated axis ratios of cloud ice particles (even their minimal values) are useful parameters of cloud microphysics.

The main conclusions of the study are as follows.

- To retrieve the parameters of cloud ice particles, the radar biases in the transmit and receive signal paths, as well as the differential phase in transmit, should be known.
- The Z_{DR} from the operational WSR-88Ds can be used to obtain areas containing platelike particles. This could be an additional output product of the system.
- Since the shapes of pristine ice particles are closer to prisms than to spheroids, the retrieved axis ratios for prisms are considered to be better values than those obtained for spheroids. The prism shape has larger retrieved axis ratios than those of spheroids. The statistical retrieval uncertainties in a/b and σ_θ are about 30%–40% at SNR > 10 dB.
- The retrieval procedure shows well-pronounced areas of certain values of the axis ratios and the degree of orientation that could be used in the interpretations of cloud processes.

Acknowledgments. The discussions with Dr. T. Schuur are greatly appreciated. Constructive comments from the anonymous reviewers helped to improve the manuscript. Funding for this study was provided in part by the NOAA/Office of Oceanic and Atmospheric Research under NOAA–University of Oklahoma Cooperative Agreement NA17RJ1227, U.S. Department of Commerce.

APPENDIX

Distributions of the Canting Angles

Distributions of θ can be described with the Gaussian, Fisher, and axial bell-shaped functions (e.g., Bringi and Chandrasekar 2001, section 2.3.6). The truncated Gaussian distribution is defined in the interval 0–π as

$$P(\theta) = D^{-1}\exp[-(\theta - \langle\theta\rangle)^2/2\sigma_\theta^2], \qquad \text{(A1)}$$
$$D = \int_0^\pi \sin\theta \exp[-(\theta - \langle\theta\rangle)^2/2\sigma_\theta^2]\,d\theta,$$

where $\langle\theta\rangle$ is the mean canting angle and σ_θ is a parameter depending on the width of the distribution. For narrow distributions, the width equals σ_θ. This distribution was used by Vivekanandan et al. (1991) and Matrosov et al. (2001), among others. At zero mean canting angle, moment J_1 from (21) is

$$J_1 = \langle\sin^2\theta\rangle = D^{-1}\int_0^\pi \sin^3\theta \exp(-\theta^2/2\sigma_\theta^2)\,d\theta. \qquad \text{(A2)}$$

Moment J_2 is obtained similarly. Distribution (A1) has been used in this study. For horizontally oriented platelike scatterers, $J_1 = J_2 = 0$, and $J_1 = J_2 = 1$ for columnar particles oriented horizontally. For the totally random distribution, $J_1 = 2/3$ and $J_2 = 8/15$. Moments

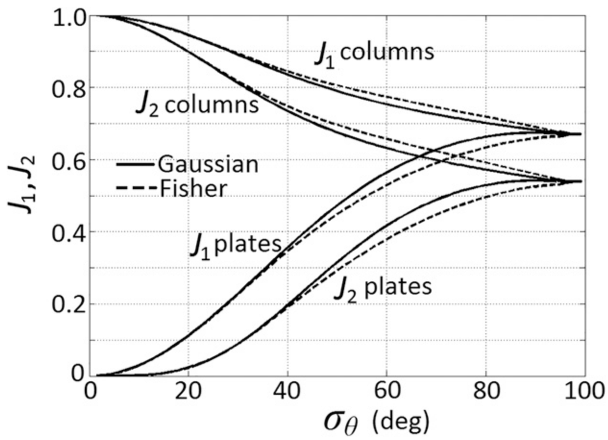

FIG. A1. Moments J_1 and J_2 as functions of the width of Gaussian (solid lines) and Fisher (dashed lines) distributions for platelike and columnar scatterers.

J_1 and J_2 as functions of the width of distribution are shown in Fig. A1 with the solid lines.

The Fisher distribution naturally describes probabilities on a sphere. For platelike particles with zero mean canting angle, $P(\theta, \varphi)$ is a function of θ only:

$$P(\theta) = \frac{\mu}{2\sinh(\mu)}\exp(\mu\cos\theta), \quad \mu \ge 0, \tag{A3}$$

where parameter μ can be represented via the width σ_θ of distribution

$$\sigma_\theta^2 = \int_0^\pi \theta^2 P(\theta)\sin\theta\, d\theta. \tag{A4}$$

For platelike particles, the moments from (21) are

$$J_1 = \frac{2}{\mu}\left(\coth\mu - \frac{1}{\mu}\right), \quad J_2 = \frac{4}{\mu^2}(2 - 3J_1). \tag{A5}$$

For columns oriented preferably horizontally, $\langle\theta\rangle = 90°$ and the Fisher distribution depends on θ and φ. In this case, averaging over θ and φ cannot be separated and moments J_1 and J_2 have been obtained numerically. This feature makes the application of the distribution cumbersome. Moments J_1 and J_2 as function of the width of distribution are shown in Fig. A1 for columnar and platelike scatterers. One can see that the difference in the moments of the Gaussian and Fisher distributions can be considered insignificant for the scattering problems under consideration.

To obtain the minimal ρ_{hv} for ice plates, (13), (16), and (19) should be used with the values corresponding to randomly oriented very thin particles, that is, $J_1 = 2/3$, $J_2 = 8/15$, $\alpha_h = V(\varepsilon - 1)$, $\Delta\alpha = -V(\varepsilon - 1)^2/\varepsilon$, and $\psi_t = 27°$ measured in KOUN. The result is $\rho_{hv} = 0.898$.

REFERENCES

Bailey, M. P., and J. Hallet, 2009: A comprehensive habit diagram for atmospheric ice crystals: Confirmation from the Laboratory, AIRS II, and other field studies. *J. Atmos. Sci.*, **66**, 2888–2899, doi:10.1175/2009JAS2883.1.

Bringi, V. N., and V. Chandrasekar, 2001: *Polarimetric Doppler Weather Radar: Principles and Applications.* Cambridge University Press, 636 pp.

Cunningham, J. G., W. D. Zittel, R. R. Lee, R. L. Ice, and N. P. Hoban, 2013: Methods for identifying systematic differential reflectivity (Zdr) biases on the operational WSR-88D network. *36th Conf. on Radar Meteorology*, Amer. Meteor. Soc., 9B.5. [Available online at https://ams.confex.com/ams/36Radar/webprogram/Paper228792.html.]

Doviak, R. J., and D. S. Zrnić, 2006: *Doppler Radar and Weather Observations*. 2nd ed. Academic Press, 562 pp.

Garrett, T. J., S. E. Yuter, C. Fallgatter, K. Shkurko, S. R. Rhodes, and J. L. Endries, 2015: Orientations and aspect ratios of falling snow. *Geophys. Res. Lett.*, **42**, 4617–4622, doi:10.1002/2015GL064040.

Gossard, E. E., and R. G. Strauch, 1983: *Radar Observations of Clear Air and Clouds*. Elsevier, 280 pp.

Görsdorf, J. U., V. Lehmann, M. Bauer-Pfundstein, G. Peters, D. Vavriv, V. Vinogradov, and V. Volkov, 2015: A 35-GHz polarimetric Doppler radar for long-term observations of cloud parameters—Description of system and data processing. *J. Atmos. Oceanic Technol.*, **32**, 675–690, doi:10.1175/JTECH-D-14-00066.1.

Ice, R. I., A. K. Heck, J. G. Cunningham, and W. D. Zittel, 2014: Challenges of polarimetric weather radar calibration. *Proc. Eighth European Conf. Radar in Meteorology and Hydrology*, Garmisch-Partenkirhen, Germany, DWD and DLR, 8.1. [Available online at http://www.pa.op.dlr.de/erad2014/programme/ExtendedAbstracts/117_Ice.pdf.]

Hogan, R. J., P. R. Field, A. J. Illingworth, A. J. Cotton, and T. W. Choularton, 2002: Properties of embedded convection in warm-frontal mixed-phase cloud from aircraft and polarimetric radar. *Quart. J. Roy. Meteor. Soc.*, **128**, 451–476, doi:10.1256/003590002321042054.

——, L. Tian, P. R. A. Brown, C. D. Westbrook, A. J. Heymsfield, and J. D. Eastment, 2012: Radar scattering from ice aggregates using the horizontally aligned oblate spheroid approximation. *J. Appl. Meteor. Climatol.*, **51**, 655–671, doi:10.1175/JAMC-D-11-074.1.

Holt, A. R., 1984: Some factors affecting the remote sensing of rain by polarization diversity radar in 3- to 35-GHz frequency range. *Radio Sci.*, **19**, 1399–1421, doi:10.1029/RS019i005p01399.

Hong, G., 2007: Parametrization of scattering and absorption properties of nonspherical ice crystals at microwave frequencies. *J. Geophys. Res.*, **112**, D11208, doi:10.1029/2006JD008364.

Hubbert, J. C., S. M. Ellis, W.-Y. Chang, S. Rutledge, and M. Dixon, 2014a: Modeling and interpretation of S-band ice crystal depolarization signatures from data obtained by simultaneously transmitting horizontally and vertically polarized fields. *J. Appl. Meteor. Climatol.*, **53**, 1659–1677, doi:10.1175/JAMC-D-13-0158.1.

——, ——, ——, and Y.-C. Liou, 2014b: X-band polarimetric observations of cross coupling in the ice phase of convective storms in Taiwan. *J. Appl. Meteor. Climatol.*, **53**, 1678–1695, doi:10.1175/JAMC-D-13-0360.1.

Kajikawa, M., 1976: Observation of falling motion of columnar snow crystals. *J. Meteor. Soc. Japan*, **54**, 276–283.

Klett, J. D., 1995: Orientation model for particles in turbulence. *J. Atmos. Sci.*, **52**, 2276–2285, doi:10.1175/1520-0469(1995)052<2276:OMFPIT>2.0.CO;2.

Kneifel, S., A. von Lerber, J. Tiira, D. Moisseev, P. Kollias, and J. Leinonen, 2015: Observed relations between snowfall microphysics and triple-frequency radar measurements. *J. Geophys. Res. Atmos.*, **120**, 6034–6055, doi:10.1002/2015JD023156.

Liu, G., 2008: A database of microwave single-scattering properties for nonspherical ice particles. *Bull. Amer. Meteor. Soc.*, **89**, 1563–1570, doi:10.1175/2008BAMS2486.1.

Mace, G. G., A. J. Heymsfield, and M. R. Poellot, 2002: On retrieving the microphysical properties of cirrus clouds using the moments of the millimeter-wavelength Doppler spectrum. *J. Geophys. Res.*, **107**, 4815–4823, doi:10.1029/2001JD001308.

Matrosov, S. Y., 2015: Evaluations of the spheroidal particle model for describing cloud radar depolarization ratios of ice hydrometeors. *J. Atmos. Oceanic Technol.*, **32**, 865–879, doi:10.1175/JTECH-D-14-00115.1.

——, R. A. Kropfli, B. E. Martner, and B. W. Bartram, 2001: On the use of radar depolarization ratios for estimating shapes of ice hydrometeors in winter clouds. *J. Appl. Meteor.*, **40**, 479–490, doi:10.1175/1520-0450(2001)040<0479:OTUORD>2.0.CO;2.

——, R. F. Reinking, and I. V. Djalalova, 2005: Inferring fall attitudes of pristine dendritic crystals from polarimetric radar data. *J. Atmos. Sci.*, **62**, 241–250, doi:10.1175/JAS-3356.1.

Melnikov, V. M., and D. S. Zrnić, 2007: Autocorrelation and cross-correlation estimators of polarimetric variables. *J. Atmos. Oceanic Technol.*, **24**, 1337–1350, doi:10.1175/JTECH2054.1.

——, and J. Straka, 2013: Axis ratios and flutter angles of cloud ice particles: Retrievals from radar data. *J. Atmos. Oceanic Technol.*, **30**, 1691–1703, doi:10.1175/JTECH-D-12-00212.1.

——, D. S. Zrnić, R. J. Doviak, P. B. Chilson, D. B. Mechem, and Y. Kogan, 2011: Prospects of the WSR-88D radar for cloud studies. *J. Appl. Meteor. Climatol.*, **50**, 859–872, doi:10.1175/2010JAMC2303.1.

Mishchenko, M. I., D. J. Wielaard, and B. E. Carlson, 1997: T-matrix computations of zenith-enhanced lidar backscatter from horizontally oriented ice plates. *Geophys. Res. Lett.*, **24**, 771–774, doi:10.1029/97GL00545.

Myagkov, A., P. Seifert, M. Bauer-Pfundstein, and U. Wandinger, 2016: Cloud radar with hybrid mode towards estimation of shape and orientation of ice crystals. *Atmos. Meas. Tech.*, **9**, 469–489, doi:10.5194/amt-9-469-2016.

Noel, V., and H. Chepher, 2004: Study of ice crystal orientation in cirrus clouds based on satellite polarized radiance measurements. *J. Atmos. Sci.*, **61**, 2073–2081, doi:10.1175/1520-0469(2004)061<2073:SOICOI>2.0.CO;2.

——, and K. Sassen, 2005: Study of planar ice crystal orientation in ice clouds from scanning polarization lidar observations. *J. Appl. Meteor.*, **44**, 653–664, doi:10.1175/JAM2223.1.

Platt, C. M. R., 1977: Lidar observations of a mixed-phase altocumulus cloud. *J. Appl. Meteor.*, **16**, 339–345, doi:10.1175/1520-0450(1977)016<0339:LOOAMP>2.0.CO;2.

——, 1978: Lidar backscatter from horizontal ice crystal plates. *J. Appl. Meteor.*, **17**, 482–488, doi:10.1175/1520-0450(1978)017<0482:LBFHIC>2.0.CO;2.

——, N. I. Abshire, and G. T. McNice, 1978: Some microphysical properties of an ice cloud from lidar observations of horizontally oriented crystals. *J. Appl. Meteor.*, **17**, 1220–1224, doi:10.1175/1520-0450(1978)017<1220:SMPOAI>2.0.CO;2.

Pruppacher, H. R., and J. D. Klett, 1997: *Microphysics of Clouds and Precipitation*. Kluwer Academic, 954 pp.

Ryzhkov, A. V., and D. S. Zrnić, 2007: Depolarization in ice crystals and its effect on radar polarimetric measurements. *J. Atmos. Oceanic Technol.*, **24**, 1256–1267, doi:10.1175/JTECH2034.1.

Teschl, F., W. L. Randeu, and R. Teschl, 2009: Single scattering from frozen hydrometeors at microwave frequencies. *Atmos. Res.*, **94**, 564–578, doi:10.1016/j.atmosres.2009.09.001.

——, ——, and ——, 2013: Single scattering of preferentially oriented ice crystals at centimeter and millimeter wavelengths. *Atmos. Res.*, **119**, 112–119, doi:10.1016/j.atmosres.2011.10.004.

Tyynelä, J., J. Leinonen, D. Moisseev, and T. Nousiainen, 2011: Radar backscattering from snowflakes: Comparison of fractal, aggregate, and soft spheroid models. *J. Appl. Meteor. Climatol.*, **28**, 1365–1372, doi:10.1175/JTECH-D-11-00004.1.

Vivekanandan, J., W. M. Adams, and V. N. Bringi, 1991: Rigorous approach to polarimetric radar modeling of hydrometeor orientation distributions. *J. Appl. Meteor.*, **30**, 1053–1063, doi:10.1175/1520-0450(1991)030<1053:RATPRM>2.0.CO;2.

Westbrook, C. D., A. J. Illingworth, E. J. O'Connor, and R. J. Hogan, 2010: Doppler lidar measurements of oriented planar ice crystals falling from supercooled and glaciated cloud layers. *Quart. J. Roy. Meteor. Soc.*, **136**, 260–276, doi:10.1002/qj.528.

——, 2014: Rayleigh scattering by hexagonal ice crystals and the interpretation of dual-polarization radar measurements. *Quart. J. Roy. Meteor. Soc.*, **140**, 2090–2096, doi:10.1002/qj.2262.

Williams, E. R., and Coauthors, 2013: End-to-end calibration of NEXRAD differential reflectivity with metal spheres. *36th Conf. on Radar Meteorology*, Breckenridge, CO, Amer. Meteor. Soc., 316. [Available online at https://ams.confex.com/ams/36Radar/webprogram/Paper228796.html.]

——, and Coauthors, 2015: Measurements of differential reflectivity in snowstorms and warm season stratiform systems. *J. Appl. Meteor. Climatol.*, **54**, 573–595, doi:10.1175/JAMC-D-14-0020.1.

Zikmunda, J., and G. Vali, 1972: Fall patterns and fall velocities of rimed ice crystals. *J. Atmos. Sci.*, **29**, 1334–1347, doi:10.1175/1520-0469(1972)029<1334:FPAFVO>2.0.CO;2.

Zrnić, D. S., V. M. Melnikov, and J. K. Carter, 2006: Calibrating differential reflectivity on the WSR-88D. *J. Atmos. Oceanic Technol.*, **23**, 944–951, doi:10.1175/JTECH1893.1.